Electron density and energy density view on the atomic interactions in SrTiO$_3$

Elizabeth A. Zhurova[a] **and**
Vladimir G. Tsirelson[b]*

[a]Department of Chemistry, University of Toledo, 2801 W. Bancroft Street, Toledo, OH 43606, USA, and [b]Mendeleev University of Chemical Technology, Miusskaya Square 9, Moscow 125047, Russia

Correspondence e-mail: tsirel@muctr.edu.ru

The results of topological analysis of the electron density in an SrTiO$_3$ crystal based on the experimental (at 145 K) and theoretical data are presented and discussed. The features of the electron density lead to the conclusion that the Ti—O interaction is of the partly polar covalent (or intermediate) type. Complicated atomic shapes defined by the zero-flux surfaces in the electron density are revealed. It is found that, in general, they are far from spherical and have very slight asphericity in the close-packed layers. The topological coordination numbers of Sr and Ti are the same as the geometrical numbers, whereas the topological coordination for the O atom (6) differs from the geometrical value (12). The latter results from the specific shape of the Ti-atom basin, which prevents bond-path formation between the O atoms. The analysis of the kinetic and potential energy densities derived from the electron density using the density functional theory formulae revealed the stabilizing crystal-forming role of the O atoms in SrTiO$_3$. Structural homeomorphism between the experimental electron density and the potential and kinetic energy densities is observed.

1. Introduction

Traditionally, the chemical bonds in cubic perovskite crystals were considered ionic (Burfoot, 1967). At the same time, Megaw (1952) noted that in order to understand the properties of perovskites, the covalent component of the chemical bond has to be taken into account. The results of first-principle calculations for cubic SrTiO$_3$ (Weyrich & Siems, 1985; Weyrich & Madenach, 1990; Xu *et al.*, 1990; Blaha & Schwarz, 1994) showed that there is a covalent component of the Ti—O bond, while the Sr—O bond has a predominantly ionic character. Using experimental Fourier-deformation electron-density maps, Buttner & Maslen (1992) and Abramov *et al.* (1995) revealed a statistically significant concentration of the electron density in the Ti—O bond. Ikeda *et al.* (1998), analyzing X-ray diffraction data by the maximum entropy method, also found a covalent component of the Ti—O bond.

Recently, Tsirelson *et al.* (2000) and Zhurova *et al.* (2000) performed a topological electron-density analysis of cubic KNiF$_3$ and KTaO$_3$ perovskites. The electron density of these crystals was reconstructed from X-ray diffraction data using the multipole model, and relatively high electron-density values of 0.50 (2) e Å^{-3} for the Ni—F bond and 1.08 (9) e Å^{-3} for the Ta—O bond were found. These bonds were associated with the intermediate atomic interaction type in terms of the Bader (1990) topological theory. In this work, we present the results of topological analysis of the experimental and theoretical electron densities in SrTiO$_3$, which provide quantitative characteristics of the atomic interactions in this compound. We will also complete the topological analysis of the electron

density with a study of the local kinetic and potential energies derived from the X-ray experimental model electron density (Tsirelson, 2000, 2002).

The cubic perovskite $SrTiO_3$ (space group $Pm\bar{3}m$) contains one molecule per unit cell. The symmetry of the Sr and Ti atomic positions is $m\bar{3}m$, while O is sited in the $4/mmm$ position. According to classical crystal chemistry, the Sr atom is geometrically coordinated with 12 O atoms, and each O atom is coordinated with four Sr and eight other O atoms. Sr and O atoms together build close-packed atomic layers, while the Ti atoms are sited in octahedral holes.

2. Topological characterization of bonding in crystals

The topological theory (Bader, 1990) is a quantum-mechanical theory that allows quantitative structural and bonding information to be obtained from the electron density. It analyzes a crystal or molecule in terms of the electron density, $\rho(\mathbf{r})$, its gradient vector field, $\nabla\rho(\mathbf{r})$, the electron-density curvature, and the critical points' positions and characteristics. Each critical point, the point where $\nabla\rho(\mathbf{r}_{CP}) = 0$, is defined by its rank and signature, i.e. the number of non-zero eigenvalues of the curvature (Hessian) matrix (λ_i) and the sum of the algebraic signs of λ_i, respectively. The electron density has four kinds of non-degenerate critical points of the rank 3: maxima $(3,-3)$, minima $(3,+3)$, and two types of saddle points $(3,+1)$ and $(3,-1)$, corresponding to the nuclear positions, cages, rings and bonds. All types of critical points are present in crystals, and their positions are restricted by the space group symmetry (Zou & Bader, 1994; Pendas et al., 1997).

Considering the $\nabla\rho(\mathbf{r})$ field, one can note pairs of gradient lines originated at the $(3,-1)$ critical point and terminating at the two neighboring nuclei. They form the atomic interaction lines along which the electron density is maximal with respect to any lateral displacement. In equilibrium, these lines are named bond paths, and associated $(3,-1)$ points are termed bond critical points. $\lambda_1 < 0$ and $\lambda_2 < 0$ at the $(3,-1)$ critical point correspond to the directions normal to the bond path and measure the degree of electron-density contraction towards this point. $\lambda_3 > 0$ measures the degree of electron-density contraction towards each of the neighboring nuclei.

The nuclei of neighboring atoms in a crystal are separated in the $\nabla\rho(\mathbf{r})$ field by surfaces of zero-flux defined by the gradient lines terminating at the $(3,-1)$ critical points. This defines these bounded atoms in terms of the electron density. All the properties of these bounded atoms are defined by the principle of stationary action; the Hohenberg–Kohn and virial theorems are valid for them (Bader, 1990, 1994).

The Laplacian of the electron density $\nabla^2\rho(\mathbf{r})$ connects the (quasi-classical) kinetic electronic energy density $g(\mathbf{r}) > 0$ and the potential electronic energy density $v(\mathbf{r}) < 0$ through the local form of the virial theorem[1] (Bader, 1990),

$$2g(\mathbf{r}) + v(\mathbf{r}) = \frac{1}{4}\nabla^2\rho(\mathbf{r}). \qquad (1)$$

It also characterizes the local concentration and depletion of electrons at each point $\mathbf{r}$ of a crystal unit cell. The sign of the Laplacian $\nabla^2\rho(\mathbf{r}_b) = \lambda_1 + \lambda_2 + \lambda_3$ at the $(3,-1)$ bond critical point depends on the relation between the principal curvatures of the electron density at $\mathbf{r}_b$, and it therefore reflects the character of the atomic interactions. If the electrons are locally concentrated around the bond critical point $[\nabla^2\rho(\mathbf{r}_b) < 0]$ then electrons are shared by both nuclei (shared interactions). This is typical for a covalent bond. The local potential energy dominates at the $(3,-1)$ critical point in this case. If electrons are concentrated in each of the atomic basins and $\nabla^2\rho(\mathbf{r}_b) > 0$, the interaction belongs to the closed-shell type. This is typical for ionic and hydrogen bonds, as well as for van der Waals interactions (Bader & Essen, 1984). Whether the kinetic or potential energy plays the dominant role in this case depends on the specificity of the atomic interactions.

The density of the total electronic energy (Bader & Beddall, 1972)

$$h_e(\mathbf{r}) = g(\mathbf{r}) + v(\mathbf{r}) \qquad (2)$$

gives an additional criterion for recognition of the atomic interaction type: $h_e(\mathbf{r}_b) < 0$ is observed for shared-type atomic interactions, while $h_e(\mathbf{r}_b) > 0$ is observed for closed-shell interactions (Cremer & Kraka, 1984; Bone & Bader, 1996).

No repulsive potential energy region exists in a system under equilibrium (Bader & Essen, 1984). For every atomic interaction type (Keith et al., 1996), a line of maximally negative potential energy density is observed linking the nuclei. The presence of a virial path between any two atoms yields a bond path between them: in other words, a virial path is homeomorphically mirrored by a bond path. The corresponding electron accumulation leads to the balancing of the Hellmann–Feynman forces and results in the equilibrium of the system. Therefore, the presence of a virial path and its associated bond path is 'an indicator of bonding between atoms' (Bader, 1998). The network of virial and bond paths linking neighboring nuclei defines a molecular graph, which is invariant to the nuclear vibrations in a stable system.

Thus, consideration of the local energies itself provides a direct approach to the study of bonding in molecules and crystals. According to Hohenberg & Kohn (1964), the electron density uniquely defines the energy of any system in its non-degenerate ground state. One way to (approximately) obtain the local energy characteristics from the electron density is to apply the density functional theory (Kirzhnits et al., 1975; Lundqvist & March, 1983; Dahl & Avery, 1984; Dreizler & Gross, 1990; Ellis, 1995; Springborg, 1997; Fuentealba, 1997). The experimental electron density might be used in the density functional theory formulae (Tsirelson, 1992). For example, the expression for the kinetic energy density based on the gradient expansion of the one-particle Green function around the classical Thomas–Fermi approximation (Kirzhnits, 1957),

$$g(\mathbf{r}) = \frac{3}{10}(3\pi^2)^{2/3}\rho(\mathbf{r})^{5/3} + \frac{1}{72}\frac{[\nabla\rho(\mathbf{r})]^2}{\rho(\mathbf{r})} + \frac{1}{6}\nabla^2\rho(\mathbf{r}), \qquad (3)$$

---

[1] Atomic units are used throughout this paper for the energy characteristics.

was used in numerous studies (Santos & Villagra, 1972; Brack *et al.*, 1976; Alonso & Girifalco, 1978; Grammaticos & Voros, 1979; Yang, 1986; Dreizler & Gross, 1990; Yang *et al.*, 1996). Following Masunov & Vyboishchikov (1993), Abramov (1997) applied (3) to model electron density in order to study the kinetic energy values at the bond critical points of some covalent and ionic compounds. Espinosa *et al.* (1998) supplemented this approach, determining the potential energy values at these critical points using the local form of the virial theorem (1).

Using theoretical and experimental electron densities, Tsirelson (2000, 2002) and Tsirelson & Ivanov (2000) have studied local energy distributions $h_e(\mathbf{r})$, $g(\mathbf{r})$ and $v(\mathbf{r})$ in crystalline systems with covalent (diamond, germanium, urea), ionic (LiF, MgO) and van der Waals (solid krypton) bonds. They found that the local virial theorem (1) is applicable to model electron densities fitted to experimental structure factors. The resulting potential energy densities are negative everywhere in all compounds studied, excluding small areas close to the nuclei where the Laplacian term in (3) diverges. Moreover, applying this approach to the model electron density leads to a kinetic energy density *quantitatively* close to the Hartree–Fock kinetic energy density (Tsirelson, 2002). The same conclusion is true for the potential energy density calculated from the model electron density *via* the local virial theorem (1). Therefore, we apply the outlined approach to study the topological and energy features of bonding in the $SrTiO_3$ crystal in this work.

3. Data treatment

The X-ray diffraction structure factors used in this work were measured up to $\sin\theta/\lambda = 1.243$ Å^{-1} at 145 (1) K with Mo $K\alpha$ radiation. All experimental details have been published by Abramov *et al.* (1995). The structural crystal model used for the treatment of the experimental data was as follows.

The electron density was approximated by the Hansen & Coppens (1978) multipole model and presented as a sum of the pseudo-atomic electron densities:

$$\rho_{\text{atomic}}(\mathbf{r}) = \rho_{\text{core}}(r) + P_v \kappa'^3 \rho_{\text{valence}}(\kappa' r)$$
$$+ \sum_{l=1}^{4} \kappa''^3 R_l(\kappa'' r) \sum_{m=-l}^{l} P_{lm} y_{lm}(\mathbf{r}/r). \quad (4)$$

Because of the high local symmetry of the atomic positions in $SrTiO_3$, only the P_v, P_{20} (only for O atoms), P_{40} and P_{44+} multipole parameters are non-zero (the multipole expansion up to the hexadecapole level, $l_{\max} = 4$, was used). The optimized parameters were the scale factor, the atomic valence-shell contraction/expansion parameters κ' and κ'', and the multipole electron populations P_v and P_{lm}. The neutral-atom wave functions by Clementi & Roetti (1974) were used to describe the core and valence electron densities. The exponential-type radial functions $r^{n_l} \exp(-\kappa'\xi r)$, with $n_l = 4, 4, 6, 8$ (Sr and Ti) and $n_l = 2, 2, 3, 4$ (O), and the values of the orbital exponents $\xi_{Sr} = 2.25$, $\xi_{Ti} = 5.43$ and $\xi_O = 4.5$ were used. The unit-cell electroneutrality condition was imposed during the

multipole refinement. The Becker & Coppens (1974) isotropic secondary extinction correction (crystal type II) found by Abramov *et al.* (1995) and the anomalous dispersion corrections from the *International Tables for Crystallography* (1995, Vol. C) were applied.

Anharmonicity of the atomic displacements was modeled with the Gram–Charlier expansion of the probability density function for atomic displacements up to tensors of the fourth rank (*International Tables for Crystallography*, 1995, Vol. C),

$$P_\mu^{\text{GC}}(\mathbf{r}) = P_\mu^{\text{harm}}(\mathbf{r})\left[1 + \left(\frac{1}{4!}\right)d^{pqrs}H_{pqrs}(\mathbf{r})\right]. \quad (5)$$

$\mathbf{r}$ is the displacement vector of an atom from its equilibrium position, $H_{pqrs}(\mathbf{r})$ are the fourth-order Hermite polynomials, d^{pqrs} are the corresponding anharmonic parameters (the third-order cumulants c^{pqr} are zero for the $m3m$ and $4/mmm$ atomic sites).

Refinements were carried out with the program *MOLDOS*97 (Protas, 1997), which is a DOS version of the program *MOLLY* (Hansen & Coppens, 1978). The procedure of the structural model refinement allowing the ED asphericity and anharmonicity of the atomic displacement to be approximately separated was as follows.

First, the scale factor and the harmonic and anharmonic atomic displacement parameters were refined with all reflections. The initial atomic valence electron populations P_v were fixed to the values obtained by Abramov *et al.* (1995) according to the Hirshfeld (1977) scheme: Sr +0.51, Ti +0.84, O −0.45 e. All the displacement parameters were refined using reflections with $\sin\theta/\lambda \geq 0.7$ Å^{-1}, and then they were fixed.

Second, the scale factor and the κ', κ'', P_v and P_{lm} parameters were refined with all reflections. The refinements were repeated until total convergence of all parameters was obtained. Special attention was paid to the control of correlations between the refined parameters; the highly correlated parameters were refined in separate groups. No correlation coefficients greater than 0.55 were observed using this method. The results were checked by the Abrahams & Keve (1971) statistical test. The final reliability factors and the refined parameters are listed in Table 1. The absence of negative regions in the total electron density (ignoring the negative sign of the electron) was taken as additional evidence of the physical significance of the results. The structure factor list is deposited.[2]

Theoretical calculation of the $SrTiO_3$ crystal based on the experimental geometry was performed by Dr Zuo with the LAPW method using the program *WIEN*97 (Blaha *et al.*, 1997). Details of the calculation are described elsewhere (Zhurova *et al.*, 2001). The generalized gradient approximation by Perdew *et al.* (1996) was used to treat exchange and correlation. The muffin-tin radius 1.80 a.u. with 581 sampling points, the plane-wave cut-off R_{MT} 1.80 a.u., $K_{\max} = 8$ and $G_{\max} = 10$ were used in the calculation. X-ray structure factors

---

Table 1
SrTiO$_3$: multipole, harmonic and anharmonic displacement parameters.

For the first six parameters, experimental results are given in the first line, while theoretical ones are listed in the second line. The atomic coordinates were Ti (0, 0, 0), O (0.5, 0, 0) and Sr (0.5, 0.5, 0.5). The reliability factors were: for the refinement over 131 experimental independent structure factors $R = 0.0053$, $R_w = 0.0048$, $S = 1.14$; for the refinement over 86 LAPW structure factors $R = 0.0039$.

Parameter	Sr	Ti	O
κ'	0.73 (3)	1.01 (3)	0.968 (3)
	0.73 (5)	1.20 (5)	0.975 (5)
$\xi\kappa''$	1.52 (9)	4.11 (9)	3.1 (3)
	1.5 (5)	5.2 (5)	2.8 (9)
P_v	1.7 (1)	2.4 (1)	6.61 (4)
	1.7 (2)	2.6 (2)	6.56 (6)
P_{20}	0	0	0.11 (3)
	0	0	0.02 (4)
P_{40}	−0.14 (9)	0.47 (8)	−0.11 (4)
	0.0 (1)	0.19 (6)	−0.07 (4)
P_{44+}	−0.10 (9)	0.35 (8)	0.08 (4)
	0.0 (1)	0.14 (6)	0.03 (4)
U_{11}	0.00356 (6)	0.0031 (1)	0.0023 (6)
U_{22}	U_{11}	U_{11}	0.0077 (3)
$d_{1111} \times 10^4$	−0.0007 (5)	−0.0011 (9)	−0.0024 (8)
$d_{2222} \times 10^4$	d_{1111}	d_{1111}	0.001 (6)
$d_{1122} \times 10^4$	−0.001 (1)	0.0000 (4)	0.001 (2)
$d_{2233} \times 10^4$	d_{1122}	d_{1122}	0.008 (4)

up to $\sin\theta/\lambda = 1.05$ Å^{-1}, calculated from the theoretical charge density, were used with the multipole model in the same way as the experimental data (except the scale factor was set to unity and displacement parameters were set to zero). The results of this multipole model refinement are also listed in Table 1 and the structure factor list is also deposited.

4. Results and discussion

The harmonic and anharmonic displacement parameters in Table 1 agree within a standard uncertainty with those reported previously by Abramov *et al.* (1995). Correspondingly, the same features of the atomic probability density functions were found, including the splitting of the oxygen position of ~0.05 Å along the Ti—O bond (the corresponding figures are deposited). Thus, the interpretation by Abramov *et al.* (1995) of the character of the atomic displacements in SrTiO$_3$, which is based on the spherical atom model, is completely confirmed when the more complicated multipole electron-density model is used instead.

The correct refinement of the atomic displacement parameters is important for the proper deconvolution of the model electron density. At the same time, there is a disagreement in the literature concerning the refinement of the anharmonic atomic displacement parameters in perovskites based on X-ray diffraction data. Jauch & Palmer (1999), using γ-ray diffraction at 111 K, and Kiat *et al.* (2000), combining synchrotron CCD data at room temperature and 120 K, synchrotron powder data at room temperature, and neutron data at room temperature, found no anharmonicity in SrTiO$_3$. In contrast, our studies of SrTiO$_3$, KTaO$_3$ (Zhurova *et al.*, 1993, 1995, 2000) and KNiF$_3$ (Ivanov *et al.*, 1999; Zhurova *et*

al., 1999) showed that if anharmonicity is significant, it could be fixed from very accurate X-ray diffraction data using adequate refinement of the structural model. Significantly, our derived atomic anharmonic probability density functions agree with the physical properties of the perovskites discussed. For example, in KNiF$_3$, which does not exhibit a structural phase transition, the probability density functions correspond to single-well atomic one-particle potentials. These latter functions have a few minima in virtual ferroelectrics SrTiO$_3$ and KTaO$_3$. This explains the possible structural transformations in these crystals with decreasing temperature. Arakcheeva *et al.* (2001) reached the same conclusion in their study of cubic Ta-bronze KTa$_{1+z}^{+(5-\delta)}$O$_3$.

Sometimes, severe extinction is mentioned as a factor smearing the probability density function's pattern (Jauch & Palmer, 2000). However, Zhurova *et al.* (1993, 1995) demonstrated that extinction, which generally distorts the anharmonic parameters' values, retains the specific pattern of the atomic anharmonic probability density functions. Therefore, perhaps some other experimental factors that are not accounted for, for example, thermal diffuse scattering, which is ignored by Jauch & Palmer (1999) and Kiat *et al.* (2000), lead to the disagreement mentioned above. We should also note that in the SrTiO$_3$ anharmonic refinement, we used thermal-diffuse-scattering corrected high-angle data measured with a point detector X-ray diffractometer [all the experimental details and primary data treatment are described by Abramov *et al.* (1995)]. Our experience with treatment of the CCD and imaging-plate data (Zhurova, 2001; Ivanov *et al.*, 1999) leads us to the conclusion that the existing methods of primary CCD data treatment do not often provide the accuracy that is necessary for anharmonic atomic displacement refinement.

The multipole parameters that we obtained were used to calculate the static model deformation electron-density maps. The program *SALLY* (Hansen, 1990) was used. The residual maps (the differences between the experimental and the dynamic multipole electron densities) showed no features greater than ± 0.1 e Å^{-3} in the interatomic space. The static deformation electron-density maps exhibit significant peaks on the Ti—O lines (Fig. 1). These peaks lie at 1.51 Å from the Ti and 0.44 Å from the O atoms and do not mimic the anharmonic smearing of the electron density, since splitting of the O atomic positions is $\sim$0.05 Å. The possible mutual influence of the multipole and anharmonic displacement parameters was minimized with the refinement procedure described above. Therefore, we can conclude that the anharmonicity of the atomic displacements and the asphericity of the valence-electron distribution in SrTiO$_3$ were reasonably separated in our structural model.

This conclusion is supported by the similarity of the model experimental and theoretical deformation electron-density maps (Fig. 1), both containing significant electron-density peaks on the Ti—O bonds. The quantitative difference in the height of these peaks results mainly from a difference between the κ'' parameters of the Ti and O atoms (Table 1). Contrary to Abramov *et al.* (1995), no significant electron-density features were found around the Sr atom in either experimental or

Table 2
Characteristics of the critical points in SrTiO₃.

For each critical point the first line lists the experimental (model) results and the second line contains the results based on the multipole refinement with theoretically calculated LAPW structure factors.

Critical point position	x	y	z	$\rho(r_{cp})$ (e Å^{-3})	$\nabla^2\rho(r_{cp})$ (e Å^{-5})	λ_1 (e Å^{-5})	λ_2 (e Å^{-5})	λ_3 (e Å^{-5})	v_{cp} (a.u.)	g_{cp} (a.u.)	$h_{e(cp)} = v_{cp}+g_{cp}$ (a.u.)	γ†	Type of critical point
$(x, 0, 0)$ Ti—O	0.2534	0.0	0.0	0.80 (7)	9.31 (8)	−4.64	−4.64	18.59	−0.196	0.144	−0.052 (3)	1.04	(3,−1)
	0.2590	0.0	0.0	0.73 (7)	9.55 (7)	−4.35	−4.35	18.28	−0.175	0.137	−0.038 (3)	1.01	
$(\frac{1}{2}, x, x)$ Sr—O	0.5	0.2333	0.2333	0.10 (2)	2.40 (3)	−0.13	−0.10	2.63	−0.014	0.019	0.006 (2)	1.04	(3,−1)
	0.5	0.2366	0.2366	0.12 (2)	2.30 (3)	−0.29	−0.19	2.78	−0.015	0.019	0.005 (2)	1.00	
(x, x, z)	0.3455	0.3455	0.1561	0.08 (2)	1.01 (3)	−0.17	0.28	0.90					(3,+1)
	0.3096	0.3096	0.1949	0.09 (2)	1.03 (4)	−0.10	0.28	0.85					
$(0, \frac{1}{2}, \frac{1}{2})$	0.0	0.5	0.5	0.05 (2)	0.32 (3)	0.06	0.13	0.13					(3,+3)
	0.0	0.5	0.5	0.05 (2)	0.31 (2)	0.08	0.11	0.12					
(x, x, x) Sr—Ti	0.2081	0.2081	0.2081	0.05 (3)	2.15 (2)	0.39	0.88	0.88					(3,+3)
	0.2592	0.2592	0.2592	0.09 (2)	0.86 (4)	0.13	0.13	0.60					

† The parameter $\gamma = \frac{1}{4}\nabla^2\rho(\mathbf{r}_{cp})/[2g(\mathbf{r}_{cp}) + v(\mathbf{r}_{cp})]$ is a criterion for the virial theorem to be fulfilled in the bond critical point: γ should be as close to unity as possible.

theoretical data (Fig. 1b). The closeness of the experimental and theoretical electron-density characteristics listed in Table 2 finally removes the question of how valid the derived topological electron-density features are.[3]

---

[3] Note that the electron density deconvoluted from atomic displacements in crystals with many well anharmonic atomic potentials does not reflect momentary changes in the covalency/ionicity of bonds resulting from atomic motion. This is a specificity pertinent to any diffraction method.
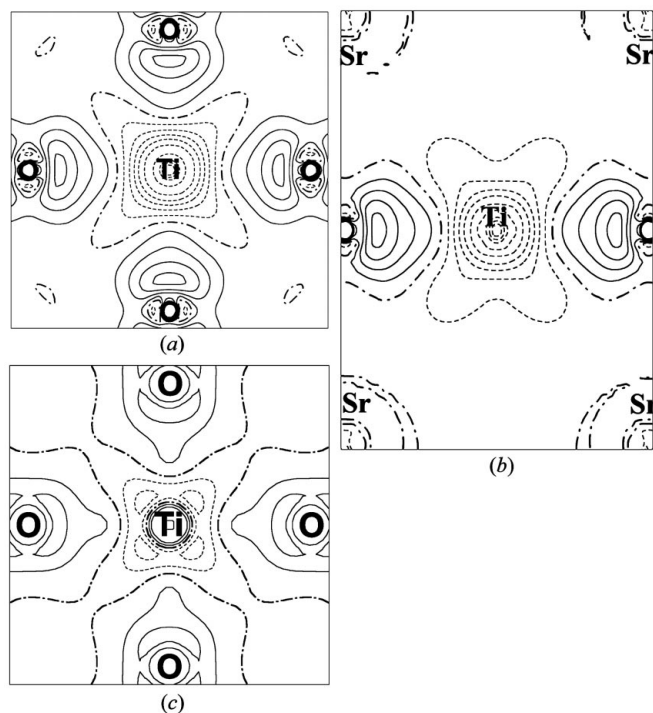
Figure 1
Static deformation electron-density maps calculated with experimental multipole parameters in the (001) plane (a) and (110) plane (b) and theoretical multipole parameters in the (001) plane (c). Contour interval is 0.1 e Å⁻³. Positive contours corresponding to an excessive electron density are solid, negative contours are dashed and the zero level is bold dash-dotted.

The total number of critical points (Table 2) obeys the Poincaré–Hopf–Morse condition (Morse & Cairns, 1969; Bader, 1990; Pendas et al., 1997). Six (3,−1) critical points on the Ti—O lines and twelve (3,−1) critical points on the Sr—O lines were found (Fig. 2). All the (3,−1) critical points in SrTiO₃ are characterized by positive values of the Laplacian of the electron density. This is an indication of the closed-shell type of interactions between the corresponding atoms (Bader, 1990). At the same time, the Ti—O and Sr—O atomic interactions are different; this difference manifests itself in the value and curvature of the electron density at the bond critical points (see Table 2). Analyzing a large body of the published topological characteristics extracted from the experimental and theoretical electron densities of different compounds, Tsirelson (1999) found that the bonds typically identified as ionic are characterized by the electron-density value at the (3,−1) critical point in the range from 0.07 to 0.25 e Å⁻³.
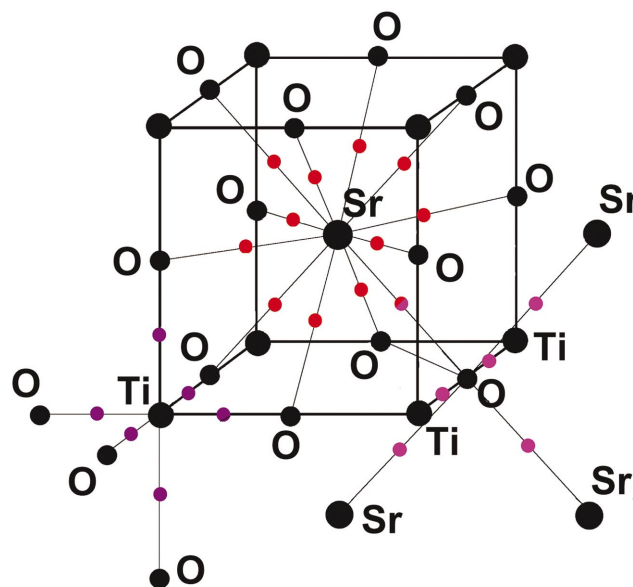
Figure 2
The atomic coordination in SrTiO₃. The bond (3,−1) critical points are shown as colored circles.

Another remarkable feature of these bonds is the specific range of the ratio of the perpendicular and parallel curvatures of the electron density: $0.12 < |\lambda|_1/\lambda_3 < 0.17$. The Sr—O interaction completely fits the first condition and, for the theoretical model, closely fits the second. Thus, the Sr—O interaction can be considered as ionic. The value and the curvatures of the electron density at the $(3,-1)$ critical point on the Ti—O line allow us to assign this bond to the *intermediate* type between the closed-shell and shared-atomic interactions. The negative sign of the electronic energy h_e at the critical points in the Ti—O bond and its positive sign for the Sr—O bond (see Table 2) support this characterization. Note that Zhurova & Tsirelson (2001) recently analyzed the features of experimental electron densities in the series of cubic perovskites and observed $h_e < 0$ at the bond critical points for the *intermediate* type of bonds and $h_e > 0$ for the closed-shell interactions in these compounds. The g_{CP} and v_{CP} values (Table 2) are about an order greater for the Ti—O bond than for the Sr—O bond. This, probably, reflects the primary energetic role of the Ti—O atomic interactions in the SrTiO$_3$ crystal formation.

The atomic shapes in SrTiO$_3$ defined by the zero-flux surfaces in the $\nabla\rho(\mathbf{r})$ field, are non-spherical to a different extent (Fig. 3a). In particular, the electron density of the easily polarized O atoms is compressed along the Ti—O line and considerably extended in the perpendicular directions. It is evident from Fig. 3(a) that it is the specific shape of the Ti atomic basin that prevents the formation of the O—O bond path and is responsible for the low oxygen coordination number. Luana *et al.* (1997) found the same shape of the B^{2+} ion basin in the series of ABC_3 perovskites having the same set of critical points as SrTiO$_3$. At the same time, in the close-packed layer of SrTiO$_3$ (Fig. 3b), the atomic shapes are only slightly aspherical. Contrary to the KNiF$_3$ crystal (Tsirelson *et al.*, 2000), where the F atomic basins are significantly separated by the Ni basins, the atomic basins of O atoms almost 'touch' each other. In spite of that, in the three-dimensional electron density there are no critical points between the O atoms and no bond paths exist. Another reason for the absence of the

O—O bond path could be the presence of the neighboring global minimum at the high symmetry $(0\frac{1}{2}\frac{1}{2})$ positions.

Abramov *et al.* (1995) stressed that in the ideal cubic perovskites ABO_3 the A—O and B—O bond lengths, R_{AO} and R_{BO}, are constrained by geometry, since each bond length is related to the lattice parameter, $\mathbf{a}$, so that $\mathbf{a} = (2R_{AO})^{1/2} = 2R_{BO}$. In general, the ratio of the values of R_{AO} and R_{BO} is not exactly $(2)^{1/2}$ and the bond lengths in cubic perovskites are stretched or compressed. These bond lengths can be predicted in the bond valence model (Brown, 1991, 1992; Brown & Altermatt, 1985). The type and size of the strain is related to the tolerance factor given by the ratio $\mathbf{a}(A)/\mathbf{a}(B)$, where $\mathbf{a}(A)$ is the lattice parameter calculated from the predicted value of R_{AO} and $\mathbf{a}(B)$ is the lattice parameter calculated from the predicted value of R_{BO}. The bonds show no strain only if $\mathbf{a}(A)/\mathbf{a}(B) = 1$: specifically, this is the case in SrTiO$_3$. As a result, this crystal occupies a special position in the series of cubic perovskites since the Sr and Ti atomic sizes are exactly matched. Consequently, SrTiO$_3$ has an undistorted cubic structure at room temperature and down to $\sim$106 K. From this point of view, the details of the close packing in SrTiO$_3$ (Fig. 3b) are especially interesting, giving a 'reference' pattern for the distorted perovskites. Comparison showed that slightly distorted KNiF$_3$ [$\mathbf{a}(A)/\mathbf{a}(B) = 1.028$] and KTaO$_3$ [$\mathbf{a}(A)/\mathbf{a}(B) = 1.086$] possess a more distinct separation between the O atomic basins (Tsirelson *et al.*, 2000; Zhurova, 2000). At the same time, the shape of the atomic basins in these crystals is approximately the same as in SrTiO$_3$.

The Laplacian (Fig. 4) demonstrates that the electron-density features are mainly concentrated around the atomic cores, where the quantum electronic shells can be seen in the vicinity of the atomic positions. The outer $3d$ and $4s$ valence electronic shells of Ti are not resolved in the $\nabla^2\rho$ distribution, as observed previously for other heavy atoms (Tsirelson & Ozerov, 1996). Note that the smaller electron depletion in the outer shell of the Ti atom along the Ti—O bond paths compared with the electron depletion in the non-bonding directions reflects the covalent component of the Ti—O bond.
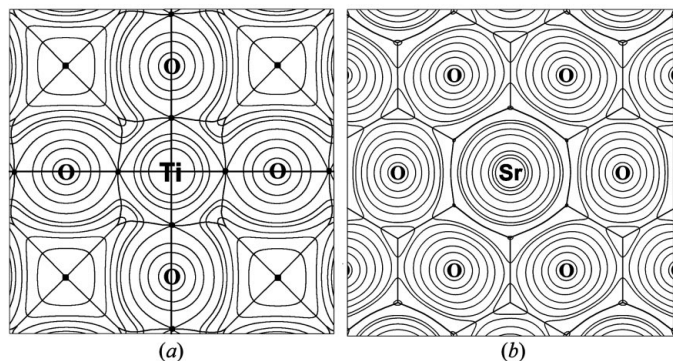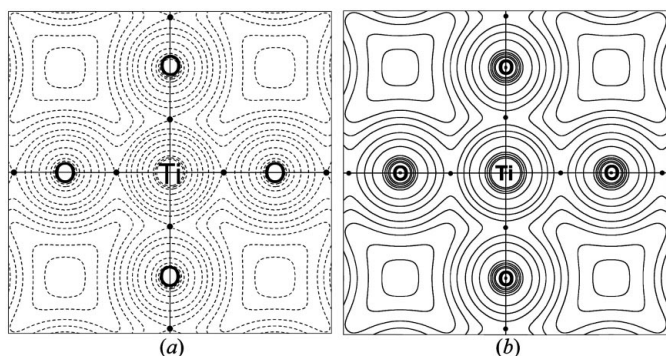

Figure 3
Experimental static total electron-density maps overlaid with the atomic zero-flux surfaces and bond paths (a) in the (001) plane and (b) in the close-packing (222) plane. $(3,-1)$ and $(3,+3)$ critical points are shown as circles and squares, respectively. Contours are 2×10^n, 4×10^n and 8×10^n e Å^{-3} ($-2 \le n \le 2$).
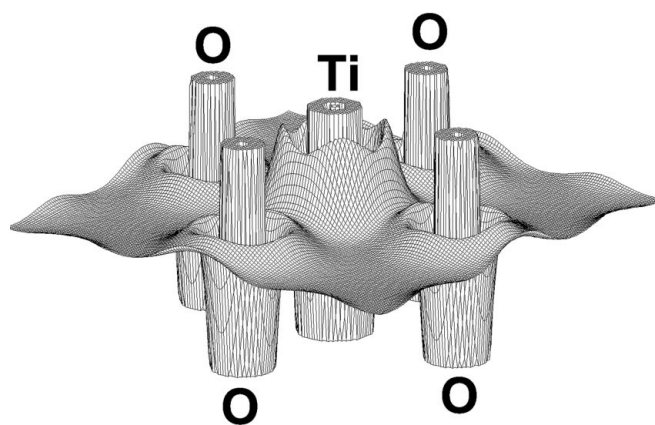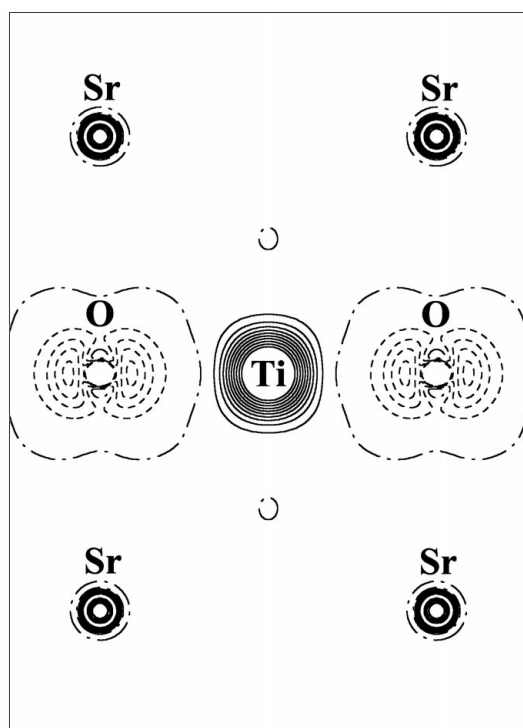

Figure 4
The experimental Laplacian of the electron density in the (001) plane. To make the $+\nabla^2\rho$ features more distinct, a non-linear vertical scale was used.

Fig. 5 contains maps of the local potential $v(\mathbf{r})$ and kinetic $g(\mathbf{r})$ energy densities overlaid with the lines of the maximally negative values of $v(\mathbf{r})$ (virial paths) and maximally positive values of $g(\mathbf{r})$. Note that the potential energy density calculated with expressions (1) and (4) is negative everywhere in

SrTiO$_3$. This demonstrates the physical significance of the energy distributions obtained, as well as the quality of the X-ray diffraction data and the electron-density modeling. Comparison of the electron density $\rho(\mathbf{r})$ (Fig. 3a) with the local potential energy (Fig. 5a) clearly shows the structural homeomorphism between these two scalar fields observed previously by Keith et al. (1996) and Bader (1998) for molecules: every bond path in the electron density is mirrored by a virial path in $-v(\mathbf{r})$. In general, the fields $\rho(\mathbf{r})$ and $g(\mathbf{r})$, and $-v(\mathbf{r})$ and $g(\mathbf{r})$, are not homeomorphic (Keith et al., 1996). However, in the particular case of SrTiO$_3$ they are homeomorphic (Figs. 3a, 5a and 5b).

The presence of the bond critical points on the interatomic lines and the (3,−1) critical points in the $-v(\mathbf{r})$ field is an indicator of the bonding interaction between the atoms (Bader, 1998). Thus, considering the corresponding bond-path network in SrTiO$_3$, we can conclude that the geometrical and topological coordination numbers of Ti and Sr are the same: 6 and 12, respectively. At the same time, in spite of the fact that the nearest Sr—O and O—O distances are the same (2.7574 Å), O is bonded to only two Ti atoms and four Sr atoms. Therefore, the topological coordination number of the O atom is 6. The same situation was found recently for the F atoms in KNiF$_3$ (Tsirelson et al., 2000).

To reveal the changes in the energy distributions caused by crystal formation, we calculated the 'deformation' potential energy density (Bader & Preston, 1969):

Figure 5
(a) The experimental potential energy density overlaid with virial paths in the (001) plane. (3,−1) critical points in the potential energy density field are shown as circles. Contours are the -2×10^n, -4×10^n and -8×10^n ($-3\le n\le2$) a.u. intervals. (b) The experimental kinetic energy density overlaid with lines of the maximum kinetic energy densities in the (001) plane. (3,−1) critical points in the kinetic energy density field are shown as circles. The contours are the 2×10^n, 4×10^n and 8×10^n ($-3\le n\le2$) a.u. intervals.
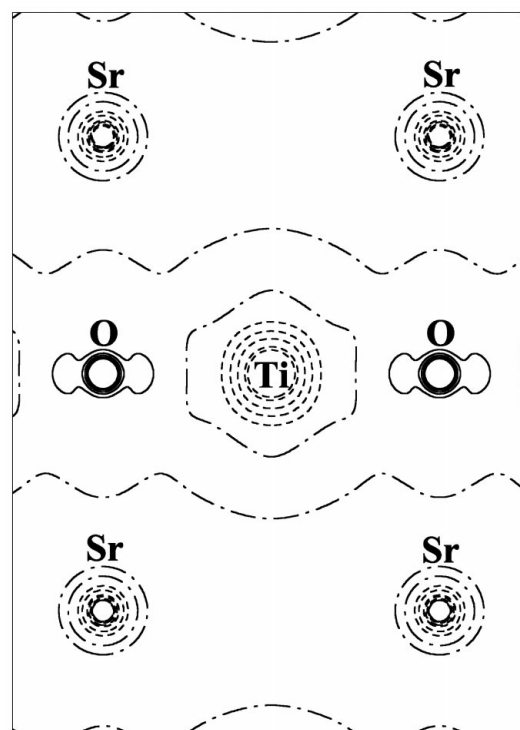

Figure 6
The experimental deformation potential energy density map in the (110) plane. Contours are $\pm2\times10^n$, $\pm4\times10^n$ and $\pm8\times10^n$ ($-3\le n\le2$) a.u. The negative contours corresponding to the enhancement of the potential energy density in the real crystal compared with the procrystal are dashed, positive contours are solid and the zero level is bold dash-dotted.

Figure 7
The experimental deformation kinetic energy density map in the (110) plane. Contours are the same as in Fig. 6. Positive lines correspond to the increase of kinetic energy density in the real crystal compared with the procrystal.

$$\delta v(\mathbf{r}) = v(\mathbf{r}) - v_{\mathrm{procrystal}}(\mathbf{r}). \tag{6}$$

Here, $v(\mathbf{r})$ is the potential energy density in a crystal, whereas $v_{\mathrm{procrystal}}(\mathbf{r})$ is the distribution of the potential energy density of the atomic procrystal (a set of spherical non-interacting atoms positioned as the real atoms in a crystal). The corresponding $\delta v(\mathbf{r})$ map calculated with the model experimental multipole parameters is shown in Fig. 6. It demonstrates that enhancement of the (negative) local potential energy in the O atomic basin and reduction of this energy in the basins of the Ti atoms accompany the formation of the $SrTiO_3$ crystal from the neutral atoms. This reveals the stabilizing role of the O atoms during the $SrTiO_3$ crystal formation. The dipole character of the deformation $v(\mathbf{r})$ distribution around the O atoms explicitly exhibits the significant polar shared contribution in the Ti—O closed-shell interaction. The redistribution of the potential energy density around the Sr atoms is practically spherical in agreement with the expected ionic interaction of these atoms with their neighbors. The general pattern of the $v(\mathbf{r})$ distribution also supports the supposition that there is no direct interaction between the Ti and Sr atoms.

The deformation kinetic energy density $\delta g(\mathbf{r}) = g(\mathbf{r}) - g_{\mathrm{procrystal}}(\mathbf{r})$ exhibits excessive kinetic energy areas around the O atoms, having significant polar deformation directed to the Ti atoms (Fig. 7). The almost spherical redistribution of the kinetic energy density around the Sr atoms takes place within the atomic basins. We summarize that all the energy-distribution features mentioned strongly support the electron-density topological characterization of the Ti—O and Sr—O bonds given above and put them on a more physical basis.

References

Abrahams, S. C. & Keve, E. T. (1971). *Acta Cryst.* A**27**, 157–165.
Abramov, Yu. A. (1997). *Acta Cryst.* A**53**, 264–272.
Abramov, Yu. A., Tsirelson, V. G., Zavodnik, V. E., Ivanov, S. A. & Brown, I. D. (1995). *Acta Cryst.* B**51**, 942–951.
Alonso, J. A. & Girifalco, L. A. (1978). *Phys. Rev. B*, **17**, 3735–3743.
Arakcheeva, A., Chapius, G., Grinevitch, V. & Shamray, V. (2001). *Acta Cryst.* B**57**, 157–162.
Bader, R. W. F. (1990). *Atoms in Molecules: A Quantum Theory.* Oxford: Clarendon Press.
Bader, R. F. W. (1994). *Phys. Rev. B*, **49**, 13348–13356.
Bader, R. F. W. (1998). *J. Phys. Chem.* A**102**, 7314–7323.
Bader, R. F. W. & Beddall, P. M. (1972). *J. Chem. Phys.* **56**, 3320–3329.
Bader, R. F. W. & Essen, H. J. (1984). *Chem. Phys.* **80**, 1943–1960.
Bader, R. F. W. & Preston, H. J. T. (1969). *Int. J. Quantum Chem.* **3**, 327–347.
Becker, P. J. & Coppens, P. (1974). *Acta Cryst.* A**30**, 129–147.
Blaha, P. & Schwarz, K. (1994). *Zeit. Kristallogr.* Suppl. **8**, S242.
Blaha, P., Schwarz, K. & Luitz, J. (1997). *Wien97.* Vienna University of Technology, Vienna, Austria.
Bone, R. G. A. & Bader, R. F. W. (1996). *J. Phys. Chem.* B**100**, 10892–10911.
Brack, M., Jennings, B. K. & Chu, Y. H. (1976). *Phys. Lett. B*, **65**, 1–4.
Brown, I. D. (1991). *Chemistry of Electronic Ceramic Materials*, edited by P. K. Davies & R. S. Roth, pp. 471–483. Washington: Department of Commerce.
Brown, I. D. (1992). *Acta Cryst.* B**48**, 553–572.
Brown, I. D. & Altermatt, D. (1985). *Acta Cryst.* B**41**, 244–247.
Burfoot, J. C. (1967). *Ferroelectrics. An Introduction to the Physical Principles.* London: D. van Nostrand Comput. Ltd.
Buttner, R. H. & Maslen, E. N. (1992). *Acta Cryst.* B**48**, 639–644.
Clementi, E. & Roetti, C. (1974). *At. Data Nucl. Data Tables*, **14**, 177–478.
Cremer, D. & Kraka, E. (1984). *Croat. Chem. Acta*, **57**, 1259–1281.
Dahl, J. P. & Avery, J. (1984). Editors. *Local Density Approximations in Quantum Chemistry and Solid State Physics.* New York: Plenum Press.
Dreizler, R. M. & Gross, E. K. U. (1990). *Density Functional Theory.* Berlin: Springer-Verlag.
Ellis, D. E. (1995). Editor. *Density Functional Theory of Molecules, Clusters and Solids.* Dordrecht: Kluwer.
Espinosa, E., Molins, E. & Lecomte, C. (1998). *Chem. Phys. Lett.* **285**, 170–173.
Fuentealba, P. (1997). *J. Phys. B*, **30**, 2039–2045.
Grammaticos, B. & Voros, A. (1979). *Ann. Phys.* **123**, 359–380.
Hansen, N. (1990). *SALLY: MS DOS Program for Calculating Static Deformation or Valence Densities.* University of Nancy I, Nancy, France.
Hansen, N. & Coppens, P. (1978). *Acta Cryst.* A**34**, 909–921.
Hirshfeld, F. L. (1977). *Theor. Chim. Acta*, **44**, 129–138.
Hohenberg, P. & Kohn, W. (1964). *Phys. Rev. B*, **136**, 864–871.
Ikeda, T., Kobayashi, T., Takata, M., Takayama, T. & Sakata, M. (1998). *Solid State Ionics*, **108**, 151.
Ivanov, Yu., Zhurova, E. A., Zhurov, V. V., Tanaka, K. & Tsirelson, V. G. (1999). *Acta Cryst.* B**55**, 923–930.
Jauch, W. & Palmer, A. (1999). *Phys. Rev. B*, **60**, 2961–2963.
Keith, T. A., Bader, R. F. W. & Aray, Y. (1996). *Int. J. Quantum Chem.* **57**, 183–198.
Kiat, J.-M., Baldinozzi, G., Dunlop, M., Malibert, C., Dkhil, B., Masson, O. & Fernandez-Diaz, M.-T. (2000). *J. Phys. Condens. Matter*, **12**, 8411–8425.
Kirzhnits, D. A. (1957). *Sov. Phys. JETP*, **5**, 64–72.
Kirzhnits, D. A., Lozovik, Yu. E. & Shpatakovskaya, G. V. (1975). *Sov. Phys. Usp.* **18**, 649–672.
Luana, V., Costales, A. & Pendas, A. M. (1997). *Phys. Rev. B*, **55**, 4285–4297.
Lundqvist, S. & March, N. H. (1983). Editors. *Theory of Inhomogeneous Electron Gas.* New York: Plenum Press.
Masunov, A. E. & Vyboishchikov, S. F. (1993). *XVI Intern. Crystallogr. Congress. Collected Abstracts*, p. 380. Beijing.
Megaw, H. D. (1952). *Acta Cryst.* **5**, 739–749.
Morse, M. & Cairns, S. S. (1969). *Critical Point Theory in Global Analysis and Differential Geometry.* New York: Academic.
Pendas, M. A., Costales, A. & Luana, V. (1997). *Phys. Rev. B*, **55**, 4275–4284.
Perdew, J. P., Burke, K. & Ernzerhof, M. (1996). *Phys. Rev. Lett.* **77**, 3865–3868.
Protas, J. (1997). *MOLDOS*96/*MOLLY.* IBM PC MS DOS updated version. University of Nancy I, Nancy, France.
Santos, E. & Villagra, A. (1972). *Phys. Rev. B*, **6**, 3134–3141.
Springborg, M. (1997). Editor. *Density-Functional Method in Chemistry and Materials Science.* Chichester: J. Wiley and Sons.
Tsirelson, V. G. (1992). *VI. Conference on Crystal Chemistry of Inorganic Compounds.* Abstracts, p. 258. L'viv, Ukraine.
Tsirelson, V. G. (1999). *Acta Cryst.* A**55** Supplement, Abstract M13.OF.003.
Tsirelson, V. G. (2000). *Russian Nat. Conf. Cryst. Chem.* Abstracts, p. 34. Chernogolovka: Institute of Problems of Chemical Physics.

Tsirelson, V. G. (2002). *Acta Cryst.* B**58**, 632–639.

Tsirelson, V. G. & Ivanov, Yu. (2000). *Sagamore XIII. Conference on Charge, Spin and Momentum Densities.* Abstracts, p. 104. Institute of Experimental Physics, Byalistok.

Tsirelson, V. G., Ivanov, Yu., Zhurova, E. A., Zhurov, V. V. & Tanaka, K. (2000). *Acta Cryst.* B**56**, 197–203.

Tsirelson, V. G. & Ozerov, R. P. (1996). *Electron Density and Bonding in Crystals.* Bristol/Philadelphia: Institute of Physics.

Weyrich, K. H. & Madenach, R. P. (1990). Ferroelectrics, **111**, 9–14.

Weyrich, K. H. & Siems, R. (1985). *Z. Phys.* B**61**, 63–68.

Xu, Y.-N., Ching, W. Y. & French, R. H. (1990). *Ferroelectrics*, **111**, 23–32.

Yang, W. (1986). *Phys. Rev. A*, **34**, 4575–4585.

Yang, Z.-Z., Liu, S. & Wang, Y. A. (1996). *Chem. Phys. Lett.* **258**, 30–36.

Zhurova, E. A. (2000). *Sagamore XIII. Conference on Charge, Spin and Momentum Densities.* Abstracts, pp. 43–44. Institute of Experimental Physics, Byalistok.

Zhurova, E. A. (2001). Unpublished.

Zhurova, E. A., Ivanov, Yu., Zavodnik, V. E. & Tsirelson, V. G. (2000). *Acta Cryst.* B**56**, 594–600.

Zhurova, E. A. & Tsirelson, V. G. (2001). Unpublished.

Zhurova, E. A., Zavodnik, V. E., Ivanov, S. A., Syrnikov, P. P. & Tsirelson, V. G. (1993). *Z. Naturforsch.* **48**a, 25–28.

Zhurova, E. A., Zavodnik, V. E. & Tsirelson, V. G. (1995). *Crystallogr. Rep.* **40**, 816–823.

Zhurova, E. A., Zhurov, V. V. & Tanaka, K. (1999). *Acta Cryst.* B**55**, 917–922.

Zhurova, E. A., Zuo, J. M. & Tsirelson, V. G. (2001). *J. Phys. Chem. Solids*, **62**, 2143–2146.

Zou, P. F. & Bader, R. F. W. (1994). *Acta Cryst.* A**50**, 714–725.